MATHEMATICS OF COMPUTATION
Volume 82, Number 281, January 2013, Pages 187–212
S 0025-5718(2012)02610-X
Article electronically published on June 5, 2012

LOCAL A POSTERIORI ERROR ESTIMATES FOR TIME-DEPENDENT HAMILTON-JACOBI EQUATIONS

BERNARDO COCKBURN, IVAN MEREV, AND JIANLIANG QIAN

Abstract. In this paper, we obtain the first local a posteriori error estimate for time-dependent Hamilton-Jacobi equations. Given an arbitrary domain Ω and a time T, the estimate gives an upper bound for the L^∞-norm in Ω at time T of the difference between the viscosity solution u and any continuous function v in terms of the initial error in the domain of dependence and in terms of the (shifted) residual of v in the union of all the cones of dependence with vertices in Ω. The estimate holds for general Hamiltonians and any space dimension. It is thus an ideal tool for devising adaptive algorithms with rigorous error control for time-dependent Hamilton-Jacobi equations. This result is an extension to the global a posteriori error estimate obtained by S. Albert, B. Cockburn, D. French, and T. Peterson in *A posteriori error estimates for general numerical methods for Hamilton-Jacobi equations. Part II: The time-dependent case*, Finite Volumes for Complex Applications, vol. III, June 2002, pp. 17–24. Numerical experiments investigating the sharpness of the a posteriori error estimates are given.

1. Introduction

In this paper, we obtain the first local a posteriori error estimate between the viscosity solution u of the following Cauchy problem for the model Hamilton-Jacobi equation,

$$u_t + H(x, \nabla u) = 0 \qquad \text{for } (x,t) \in \mathbb{R}^d \times (0,T), \tag{1.1}$$

$$u(x, t=0) = u_0(x) \qquad \text{for } x \in \mathbb{R}^d, \tag{1.2}$$

and any continuous function v. The estimate has the form

$$\| u(T) - v(T) \|_{L^\infty(\Omega)} \le \Phi(v; T, \Omega), \tag{1.3}$$

where T is an arbitrary positive number, Ω is an arbitrary sub-domain of $\mathbb{R}^d$, and as expected, the functional Φ depends on the error in the domain of dependence at the initial time and on the (shifted) residual of the function v on the union of all cones of dependence with vertices in Ω. The results in this paper extend those obtained in [2] and [3]. Indeed, when $\Omega = \mathbb{R}^d$, our estimate becomes the global estimate obtained in [3], which was in turn obtained by extending to the time-dependent case the estimate for the steady-state case proposed in [2].

Received by the editor May 7, 2010 and, in revised form, May 27, 2011.
2010 *Mathematics Subject Classification.* Primary 65M15, 65M12; Secondary 49L25.
Key words and phrases. A posteriori error estimates, Hamilton-Jacobi equations.
The first author was partially supported by the National Science Foundation (Grant DMS-0712955) and by the Minnesota Supercomputing Institute.
The third author was partially supported by the National Science Foundation (NSF 0810104 and NSF 0830161).

Several authors have obtained error estimates in the L^∞-norm for Hamilton-Jacobi equations, but the results obtained in [2] and [3], and, hence, the result in this paper, are different in many aspects. Crandall and Lions [9] obtained an a priori estimate for the difference between the viscosity solution u and the approximation v given by a monotone scheme defined on Cartesian grids. In our setting their result can be written in the form

$$\| u(T) - v(T) \|_{L^\infty(\Omega)} \leq C\sqrt{\Delta x}, \tag{1.4}$$

where Δx is the maximum mesh size and $C > 0$ is a constant. Souganidis [15] extended this estimate to more general Hamiltonians and to general finite difference schemes on Cartesian grids. Abgrall [1] introduced the intrinsic monotone schemes for unstructured meshes and proved that the same error estimate holds. Falcone and Ferretti [10] obtained a priori error estimates for Hamilton-Jacobi-Bellman equations for schemes that were constructed by using the discrete dynamic programming principle and were devised to converge very fast to the exact solution. They assume that the viscosity solution is very smooth, however, and their results apply only to convex Hamiltonians. Qian [14] proved that (1.4) holds for a modification of the classic Lax-Friedrichs scheme that allows for locally varying time and space grids.

All these a priori error estimates depend on the numerical method used to compute the approximate solution v, involve information that is *not known* about the exact solution, and cannot capture the features of the *particular* problem under consideration. In contrast, the a posteriori error estimate (1.3), as well as the a posteriori error estimates obtained in [2] and [3], hold regardless of how v is computed. They can thus be applied if v is obtained by means of a finite difference scheme such as the ENO scheme developed by Osher and Shu [13], a finite element method such as the discontinuous Galerkin (DG) method proposed by Hu and Shu [11], the Petrov-Galerkin method used by Barth and Sethian [4], or a finite volume method such as the intrinsic monotone scheme of Abgrall [1]. These estimates are also independent of the smoothness of the exact solution and take into account the particularities of the specific problem. This makes them an ideal tool for devising adaptive algorithms with rigorous error control for Hamilton-Jacobi equations.

The steady-state a posteriori error estimate obtained in [2] has been utilized in a few adaptive schemes. An adaptive method for one- and two-dimensional steady state Hamilton-Jacobi equations using a monotone scheme was developed in [6] and [7]. An adaptive scheme for steady-state Hamilton-Jacobi equations using the discontinuous Galerkin (DG) method was proposed in [5]. An adaptive method for the time-dependent case is a subject that will be explored in a forthcoming paper.

The paper is organized as follows. We state and prove the local a posteriori error estimate in section 2. In this section we follow [3] closely. We devote section 3 to the numerical study of the efficiency of the a posteriori error estimate when the approximate solution v is computed using a monotone scheme. Finally, we end in section 4 with some concluding remarks.

2. A posteriori error estimates

2.1. **The viscosity solution.** We begin by recalling the definition of the viscosity solution. To state the definition, we need the notion of *semi-differentials* of a function defined on $\mathbb{R}^d \times (0, T)$. The *superdifferential* $D^+u(x, t)$ of a function u at

a point $(x,t) \in \mathbb{R}^d \times (0,T)$ is the set of all vectors $p = (p_x, p_t)$ in $\mathbb{R}^d \times \mathbb{R}$ such that

$$\limsup_{(y,s)\in\mathbb{R}^d\times(0,T)\to(x,t)} \left(\frac{u(y,s) - \{u(x,t) + (s-t)\,p_t + (y-x)\cdot p_x\}}{\|\,(y,s)-(x,t)\,\|} \right) \le 0,$$

and the *subdifferential* $D^- u(x,t)$ of u at a point $(x,t) \in \mathbb{R}^d \times (0,T)$ is the set of all vectors $p = (p_x, p_t)$ in $\mathbb{R}^d \times \mathbb{R}$ such that

$$\liminf_{(y,s)\in\mathbb{R}^d\times(0,T)\to(x,t)} \left(\frac{u(y,s) - \{u(x,t) + (s-t)\,p_t + (y-x)\cdot p_x\}}{\|\,(y,s)-(x,t)\,\|} \right) \ge 0.$$

The definition of the viscosity solution of (1.1), (1.2) is stated in terms of the residual, which is defined as

$$R(x,p) = p_t + H(x,p_x).$$

Definition 2.1 ([8])**.** A viscosity solution u of the initial-value problem for the Hamilton-Jacobi equation (1.1), (1.2) is a continuous function on $\mathbb{R}^d \times (0,T)$ satisfying $u(x,t=0) = u_0(x)$ such that, for all (x,t) in $\mathbb{R}^d \times (0,T)$,

$$\sigma R(x,p) \le 0, \qquad \forall p \in D^\sigma u(x,t),\ \sigma \in \{+,-\}.$$

2.2. **The a posteriori error estimate.** Given any sub-domain Ω of $\mathbb{R}^d$ and any time $T > 0$, the local a posteriori error estimate that we propose gives an upper bound for the semi-norms

$$\begin{aligned} |\,u-v\,|_{-,\Omega,T} &= \sup_{x\in\Omega} \left(u(x,T) - v(x,T)\right)^+, \\ |\,u-v\,|_{+,\Omega,T} &= \sup_{x\in\Omega} \left(v(x,T) - u(x,T)\right)^+, \end{aligned}$$

in terms of the behavior of the function v on the set

$$Q_T = \bigcup_{t\in(0,T)} \Omega_{V(T-t)} \times \{t\},$$

where

$$\Omega_{Vt} = \{x :\ \mathrm{dist}(x,\Omega) \le Vt\},$$

and in terms of the quantity $|\,u-v\,|_{\sigma,\Omega_{VT},0}$. The positive parameter V is defined as

$$V = \sup_{x\in\mathbb{R}^d} |\,H(x,\cdot)\,|_{\mathrm{Lip}}, \tag{2.5}$$

where the right-hand side is assumed to be finite. This ensures that if a characteristic hits the border of Q_T, it does not enter into Q_T. Moreover, Q_T is nothing but (the intersection with $\mathbb{R}^d \times (0,T)$ of) the union of the cones of dependence with vertices in Ω; see Figure 1 below.

In order to give the statement and the proof of the error estimate, we need to introduce the following notation. For any vector $p = (p_x, p_t) \in \mathbb{R}^d \times \mathbb{R}$ and $\epsilon = (\epsilon_x, \epsilon_t)$ with $\epsilon_x, \epsilon_t > 0$, the shifted residual R_ϵ is defined as

$$R_\epsilon(x,p) = p_t + H(x - \epsilon_x p_x, p_x). \tag{2.6}$$

For $\kappa = (\kappa_x, \kappa_t) \in \mathbb{R}^2$, the paraboloid P_v is given by

$$P_v(x,t,p,\kappa;y,s) = v(x,t) + (y-x, s-t)\cdot p + \frac{\kappa_t}{2}|\,s-t\,|^2 + \frac{\kappa_x}{2}|\,y-x\,|^2, \tag{2.7}$$

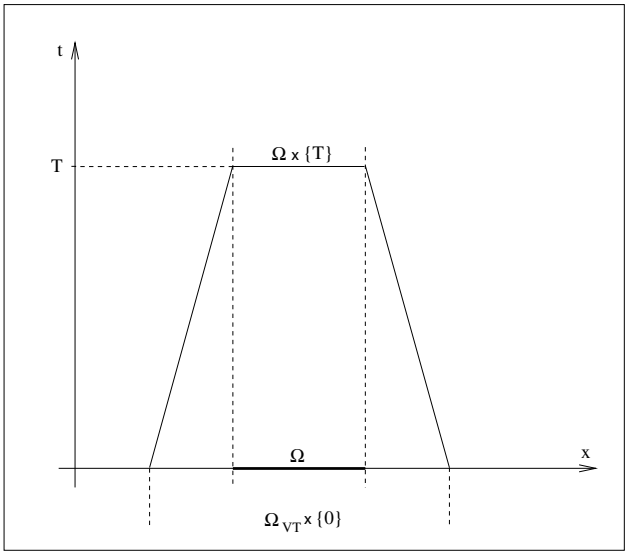

FIGURE 1. The region enclosed by the trapezoid Q_T. The viscosity solution u in $\Omega \times \{T\}$ does not depend on its initial values outside of Ω_{VT}.

for all $(y, s) \in \mathbb{R}^d \times [0, T]$. We also need the quantity

$$\omega_\epsilon(v; x, t, p) = v(x, t) - v(x - \epsilon_x p_x, 0) - \frac{\epsilon_x}{2} |\, p_x \,|^2 - \frac{t^2}{2\epsilon_t}. \tag{2.8}$$

The quantity ω_ϵ incorporates into the estimate information about the smoothness of the function v. It can be bounded in terms of the moduli of continuity of v. For example, if $v(t = 0) \in W^{1,\infty}(\mathbb{R}^d)$ and $v_t \in L^\infty(0, T; \mathbb{R}^d)$,

$$|\, \omega_{\sigma\epsilon}(v; x, t, p) \,| \le \frac{|\, v_t \,|^2_{L^\infty(0,T;\mathbb{R}^d)}}{2} \epsilon_t + \frac{|\, v(0) \,|^2_{W^{1,\infty}(\mathbb{R}^d)}}{2} \epsilon_x. \tag{2.9}$$

With the notation introduced above, we have the following result.

Theorem 2.2. *Let u be the viscosity solution of the problem* (1.1), (1.2) *and let v be any continuous function on $\mathbb{R}^d \times [0, T]$. Let Ω be a sub-domain of $\mathbb{R}^d$. Then, for $\sigma \in \{-, +\}$, we have that*

$$|\, u - v \,|_{\sigma,\Omega,T} \le |\, u - v \,|_{\sigma,\Omega_{VT},0} + \inf_{\epsilon_x, \epsilon_t > 0} \Phi_\sigma(v; \epsilon), \tag{2.10}$$

where

$$\Phi_\sigma(v; \epsilon) = \sup_{((x,t),p) \in \mathcal{A}_\sigma(v;\epsilon)} \left\{ \big(\sigma\, \omega_{\sigma\epsilon}(v; x, t, p)\big)^+ + \big(\sigma\, T\, R_{\sigma\epsilon}(x, p)\big)^+ \right\}. \tag{2.11}$$

The set $\mathcal{A}_\sigma(v; \epsilon)$ is the set of points $((x, t), p)$ in $\overline{Q_T} \times \mathbb{R}^{d+1}$ such that

$$\sigma \left\{ v(y, s) - P_v(x, t, p, (\sigma/\epsilon_x, \sigma/\epsilon_t)\,;\, y, s) \right\} \le 0 \qquad \forall (y, s) \in \overline{Q_T}. \tag{2.12}$$

Remark 1. As stated in the introduction, the above estimate reduces to the global a posteriori error estimate obtained in [3] when $\Omega = \mathbb{R}^d$.

Remark 2. Note that since

$$\max_{\sigma=\{-,+\}} |\, h \,|_{\sigma,\Omega,T} = \| \, h(x,T) \, \|_{L^\infty(\Omega)},$$

from the estimates of the semi-norms $|\, u - v \,|_{\sigma,\Omega,T}$, we obtain

$$\| \, u(x,T) - v(x,T) \, \|_{L^\infty(\Omega)} \leq \| \, u(x,0) - v(x,0) \, \|_{L^\infty(\Omega_{VT})} + \max_{\sigma\in\{-,+\}} \inf_{\epsilon_x,\epsilon_t>0} \Phi_\sigma(v;\epsilon).$$

When v satisfies certain smoothness conditions, such as the conditions required for (2.9) to hold or v is Lipschitz in both variables, we can let ϵ_x and ϵ_t go to zero in (2.10); using (2.9), we obtain

$$|\, u - v \,|_{\sigma,\Omega,T} \leq |\, u - v \,|_{\sigma,\Omega_{VT},0} + \sup_{((x,t),p)\in\overline{Q_T}\times D^\sigma v(x,t)} \left(\sigma \, T \, R(x,p)\right)^+,$$

which furthermore implies that

$$\| \, u(x,T) - v(x,T) \, \|_{L^\infty(\Omega)} \leq \| \, u(x,0) - v(x,0) \, \|_{L^\infty(\Omega_{VT})} + \max_{\sigma\in\{-,+\}} \left\{ \sup_{((x,t),p)\in\overline{Q_T}\times D^\sigma v(x,t)} \left(\sigma \, T \, R(x,p)\right)^+ \right\}.$$

This estimate is sharp when the viscosity solution u is smooth and v has a non-oscillatory residual, as will be seen from the numerical experiments. However, for a nonsmooth viscosity solution u, the right-hand side of the above inequality might remain of order one while v converges to the viscosity solution [2].

Remark 3. The point $((x,t),p)$ belongs to the set $A_-(v;\epsilon)$ if the graph of v remains above the paraboloid $P_v(x,t,p,(-1/\epsilon_x,-1/\epsilon_t);\cdot,\cdot)$. Since the paraboloid touches v at (x,t), when (x,t) is in the interior of Q_T, p belongs to $D^- v(x,t)$. This so-called **paraboloid test**, i.e., testing whether $((x,t),p)$ belongs to $A_\sigma(v;\epsilon)$, can be used to detect the location of the discontinuities in the gradient of the exact solution u at any time $t \in [0,T]$. Consider a viscosity solution u that has a kink at the point (x_0,t_0), for example. Let v be a smooth function that is, roughly speaking, "very close" to the viscosity solution u. For a given value of the auxiliary parameter $\epsilon = (\epsilon_x,\epsilon_t)$, there is an interval around (x_0,t_0) such that the points inside this interval fail the paraboloid test. We illustrate this fact when we discuss the results of our numerical experiments for nonsmooth viscosity solutions.

Remark 4. We also want to stress the role played by the auxiliary parameter $\epsilon = (\epsilon_x,\epsilon_t)$. The set $A_\sigma(v;\epsilon)$ decreases as each of the components of the auxiliary parameter ϵ increases. This induces a tendency on $\Phi_\sigma(v;\epsilon)$ to decrease. At the same time, the shifted residual $\sigma R_{\sigma\epsilon}(x,p)$ might increase. The optimal value of ϵ is obtained by balancing these two tendencies.

Remark 5. Let us argue why it is reasonable to expect that our a posteriori error estimate holds when the trapezoidal domain Q_T is *replaced* by a smaller set we denote by $\Gamma_{\Omega,T}$.

Let us motivate the definition of $\Gamma_{\Omega,T}$. From the theory of characteristics we know that the region enclosed by the trapezoid Q_T is larger than the smallest compact domain that contains the characteristics of the initial-value problem (1.1), (1.2) that enter into Ω at time T or prior to time T have entered into a shock that is inside Ω at time T. We denote this compact domain by $\Gamma_{\Omega,T}$. It is evident from equations (2.11) and (2.12) that the larger the region enclosed by the trapezoid Q_T, the larger the error estimate. This is especially true in the case when the

viscosity solution is smooth inside Ω, but the trapezoid Q_T contains a part of the path of the kink in the viscosity solution, as would be illustrated by the numerical experiments. Since the viscosity solution in Ω at time T is completely determined by the initial condition in the domain of dependence of Ω and its behavior along the characteristics that enter into Ω at time T, it is reasonable to expect that a sharper error estimate would be obtained if we replace the trapezoid Q_T by a smaller compact domain that better approximates $\Gamma_{\Omega,T}$.

We could determine the set $\Gamma_{\Omega,T}$ by solving a Hamilton-Jacobi initial-value problem. The idea is as follows. Assume that the Hamiltonian function $H(x,p)$ is differentiable with respect to p, and assume that the viscosity solution u of the initial-value problem (1.1), (1.2) has a gradient at all points $(x,t) \in \mathbb{R}^d \times (0,T)$. Now, let $\varphi(x,t)$ be the solution to the terminal-value problem

$$\varphi_t + \nabla_p H(x, \nabla u) \cdot \nabla \varphi = 0 \quad \text{for } (x,t) \in \mathbb{R}^d \times (0,T), \tag{2.13}$$
$$\varphi(x,T) = \begin{cases} 1 & \text{for } x \in \Omega, \\ 0 & \text{for } x \notin \Omega. \end{cases}$$

It is easily seen that the characteristics of (2.13) are also characteristics of (1.1) for $t \in [0,T]$. The solution to (2.13) is equal to 0 along the characteristics that are outside Ω at time T and is equal to 1 along the characteristics inside the domain $\Gamma_{\Omega,T}$.

Since u is not known a priori, to approximate the set $\Gamma_{\Omega,T}$, we could replace u by an approximation v obtained using a numerical scheme such as the Lax-Friedrichs scheme [9]. Then, we would solve (2.13) numerically to obtain an approximate solution φ_h and approximate $\Gamma_{\Omega,T}$ by the domain where φ_h is nonzero. As we are going to see, our numerical experiments do confirm that this approach works very well. The theoretical justification of the algorithm, however, is still an open problem.

2.3. **Proof of the a posteriori error estimate.** The proof we present next is a modification of the one presented in [3] for the case $\Omega = \mathbb{R}^d$. We only prove the result for $\sigma = -$ since the proof for $\sigma = +$ is entirely analogous. We proceed in several steps.

Step 1 (The auxiliary quantity Δ_δ). Note that Definition 2.1 of the viscosity solution holds only in the interior of Q_T. So instead of working with the quantity

$$\Delta = \sup_{(x,t)\in Q_T} (u(x,t) - v(x,t)) - |\, u - v \,|_{-,\Omega_{VT},0},$$

we consider the auxiliary quantity

$$\Delta_\delta = \sup_{(x,t)\in Q_T} \left(u(x,t) - v(x,t) - \frac{\delta}{\Psi(x,t)} \right) - |\, u - v \,|_{-,\Omega_{VT},0},$$

where δ is an arbitrary positive parameter,

$$\Psi(x,t) = T - t - \phi(x),$$

and the function ϕ is constructed in such a way that $\Psi(x,t) > 0$ in the interior of Q_T and that $\Psi(x,t) = 0$ for (x,t) in the set $\partial Q_T \setminus \Omega_{VT} \times \{0\}$.

It is not difficult to see that the function ϕ is nothing but the (suitably scaled) distance function to the set Ω. More precisely, ϕ is identically equal to zero in Ω,

and outside Ω, it is the viscosity solution of the eikonal equation

$$V \mid \nabla\phi(x) \mid -1 = 0 \qquad \text{for } x \in \Omega^c,$$
$$\phi(x) = 0 \qquad \text{for } x \in \partial\Omega.$$

Clearly, for $t \in [0,T]$, we have

$$\Omega_{V(T-t)} = \{x \in \mathbb{R}^d \mid \Psi(x,t) > 0\}. \tag{2.14}$$

Step 2 (The auxiliary quantity $\Delta_{\delta,\nu}$). In order to avoid some technical difficulties originating from the fact that ϕ may not be differentiable, we are going to replace it by a smoother function. To do so, we choose a smooth, nonnegative function η with integral equal to one and support in the unit ball and consider the function

$$\phi_\nu = \eta_\nu * \phi,$$

where $\eta_\nu(x) = \frac{1}{\nu^d}\,\eta(\frac{x}{\nu})$ for all $\nu > 0$, and $*$ denotes the convolution with respect to x. Clearly, ϕ_ν is a smooth function. Accordingly, we replace $\Psi(x,t)$ by $\Psi_\nu(x,t) = T - t - \phi_\nu(x)$.

Now, instead of considering the quantity Δ_δ, we take

$$\Delta_{\delta,\nu} = \sup_{(x,t)\in Q_{T,\nu}} \left(u(x,t) - v(x,t) - \frac{\delta}{\Psi_\nu(x,t)} \right) - \mid u - v \mid_{-,\Omega_{VT},0},$$

where

$$Q_{T,\nu} = \{(x,t) \in \mathbb{R}^d \times (0,T) \mid \Psi_\nu(x,t) > 0\}. \tag{2.15}$$

Note that for every $(x,t) \in Q_T$ we can write

$$u(x,t) - v(x,t) \le \mid u - v \mid_{-,\Omega_{VT},0} + \Delta_{\delta,\nu} + \frac{\delta}{\Psi_\nu(x,t)}, \tag{2.16}$$

for some $\nu < \nu_0$, $\nu_0 > 0$, because of the definitions of Q_T and $Q_{T,\nu}$, (2.14) and (2.15), and the fact that $\lim_{\nu\downarrow 0} \phi_\nu(x) = \phi(x)$ for all $x \in \mathbb{R}^d$ since ϕ is continuous.

The idea of the proof is to obtain an estimate of the form

$$\Delta_{\delta,\nu} \le C \quad \forall \delta \le \delta_0,$$

for some constants $C \ge 0$ and $\delta_0 > 0$. If we then let $\delta \to 0$ in (2.16), we obtain the desired result, namely,

$$\mid u - v \mid_{-,\Omega,T} \le \mid u - v \mid_{-,\Omega_{VT},0} + C. \tag{2.17}$$

Step 3 (The auxiliary function ψ). Assume now that for some $\delta > 0$ and $\nu > 0$, $\Delta_{\delta,\nu} > 0$; otherwise, there is nothing to prove. We introduce the auxiliary function $\psi(x,t;y,s)$ defined by

$$\psi(x,t;y,s) = u(x,t) - v(y,s) - \frac{\delta}{\Psi_\nu(x,t)} - (1-\theta)\frac{(t+s)}{2\,T}\Delta_{\delta,\nu}$$
$$- \frac{(t-s)^2}{2\epsilon_t} - \frac{|x-y|^2}{2\epsilon_x},$$

where $\theta \in (0,1)$ is a parameter to be determined later. Since both u and v are continuous and $Q_{T,\nu}$ is bounded, there exists a point $(\hat{x},\hat{t};\hat{y},\hat{s}) \in \overline{Q_{T,\nu}} \times \overline{Q_{T,\nu}}$ such that

$$\psi(\hat{x},\hat{t};\hat{y},\hat{s}) \ge \psi(x,t;y,s) \qquad \forall\, (x,t;y,s) \in \overline{Q_{T,\nu}} \times \overline{Q_{T,\nu}}. \tag{2.18}$$

Note that by definition of $Q_{T,\nu}$, (2.15), $\Psi_\nu(x,t) \geq 0$ for all the points $(x,t) \in \overline{Q_{T,\nu}}$. Since $\Psi_\nu(\hat{x},\hat{t})$ cannot be equal to zero, we must have that $\Psi_\nu(\hat{x},\hat{t}) > 0$. This implies that either $(\hat{x},\hat{t})$ belongs to the domain $Q_{T,\nu}$ or $\hat{t} = 0$.

Moreover, if we set

$$\hat{p} = (\hat{p}_y, \hat{p}_s) = \left(\frac{(\hat{x} - \hat{y})}{\epsilon_x}, -\frac{(1-\theta)}{2\,T}\Delta_{\delta,\nu} + \frac{(\hat{t} - \hat{s})}{\epsilon_t} \right),$$

the point $((\hat{y},\hat{s}),\hat{p})$ belongs to the set $\mathcal{A}_-(v;\epsilon)$. Indeed, taking $t = \hat{t}$ and $x = \hat{x}$ in (2.18), we obtain

$$\begin{aligned} v(y,s) &\geq v(\hat{y},\hat{s}) + \hat{p}\cdot(y-\hat{y}, s-\hat{s}) - \frac{1}{2\epsilon_t}|\, s-\hat{s}\,|^2 - \frac{1}{2\epsilon_x}|\, y-\hat{y}\,|^2 \\ &= P_v(\hat{y},\hat{s},\hat{p},(-1/\epsilon_t, -1/\epsilon_x); y, s). \end{aligned}$$

Step 4 (The case $\hat{t} > 0$). Assume that $\hat{t} > 0$. In this case, since the mapping $(x,t) \mapsto \psi(x,t;\hat{y},\hat{s})$ attains a maximum at $(\hat{x},\hat{t}) \in Q_{T,\nu}$, we have that

$$\begin{aligned} 0 \in D^+_{x,t}\psi(\hat{x},\hat{t};\hat{y},\hat{s}) = D^+u(\hat{x},\hat{t}) &- \left(0, \frac{(1-\theta)}{T}\Delta_{\delta,\nu}\right) \\ &+ \frac{\delta}{\Psi^2_\nu(\hat{x},\hat{t})}\left(\nabla\Psi_\nu(\hat{x},\hat{t}), \partial_t\Psi_\nu(\hat{x},\hat{t})\right) - \hat{p}. \end{aligned}$$

Hence,

$$-\frac{\delta}{\Psi^2_\nu(\hat{x},\hat{t})}\left(\nabla\Psi_\nu(\hat{x},\hat{t}), \partial_t\Psi_\nu(\hat{x},\hat{t})\right) + \left(0, \frac{(1-\theta)}{T}\Delta_{\delta,\nu}\right) + \hat{p} \in D^+u(\hat{x},\hat{t}).$$

Since u is the viscosity solution, Definition 2.1 implies that

$$-\frac{\delta}{\Psi^2_\nu(\hat{x},\hat{t})}\partial_t\Psi_\nu(\hat{x},\hat{t}) + \frac{(1-\theta)}{T}\Delta_{\delta,\nu} + \hat{p}_s + H\left(\hat{x}, \hat{p}_y - \frac{\delta}{\Psi^2_\nu(\hat{x},\hat{t})}\nabla\Psi_\nu(\hat{x},\hat{t})\right) \leq 0,$$

which can be written as

$$\frac{(1-\theta)}{T}\Delta_{\delta,\nu} \leq -\hat{p}_s - H(\hat{x},\hat{p}_y) + \Theta, \tag{2.19}$$

where

$$\Theta = \frac{\delta}{\Psi^2_\nu(\hat{x},\hat{t})}\partial_t\Psi_\nu(\hat{x},\hat{t}) + H(\hat{x},\hat{p}_y) - H\left(\hat{x}, \hat{p}_y - \frac{\delta}{\Psi^2_\nu(\hat{x},\hat{t})}\nabla\Psi_\nu(\hat{x},\hat{t})\right).$$

Next, we show that $\Theta \leq 0$. Indeed, by the definition of the parameter V, (2.5),

$$\Theta \leq \frac{\delta}{\Psi^2_\nu(\hat{x},\hat{t})}\partial_t\Psi_\nu(\hat{x},\hat{t}) + V\frac{\delta}{\Psi^2_\nu(\hat{x},\hat{t})}|\,\nabla\Psi_\nu(\hat{x},\hat{t})\,|.$$

Using the fact that

$$\left(\nabla\Psi_\nu(\hat{x},\hat{t}), \partial_t\Psi_\nu(\hat{x},\hat{t})\right) = \left(-\nabla\phi_\nu(\hat{x}), -1\right),$$

we obtain

$$\Theta \leq -\frac{\delta}{\Psi^2_\nu(\hat{x},\hat{t})}\left(1 - V|\,\nabla\phi_\nu(\hat{x})\,|\right).$$

Since

$$V\,|\,\nabla\phi_\nu(x)\,| \leq 1 \qquad \forall\, x \in \mathbb{R}^d, \tag{2.20}$$

we conclude that $\Theta \leq 0$. To see that the above inequality holds, it suffices to realize that the definition of ϕ implies that $\nabla\phi = 0$ in Ω, and that outside Ω, ϕ is

$1/V$ times the distance-to-Ω function. This implies that all the elements p of its superdifferential and subdifferential yield $V\,|\,p\,|\leq 1$. Inequality (2.20) is a reflection of this simple fact.

Since $\Delta_{\delta,\nu}>0$ and $\hat{x}=\hat{y}+\epsilon_x\hat{p}_y$, using (2.19) we obtain

$$\Delta_{\delta,\nu}\leq\frac{T}{1-\theta}\left(-\hat{p}_s-H(\hat{y}+\epsilon_x\hat{p}_y,\hat{p}_y)\right)^+,$$

which implies that

$$\Delta_{\delta,\nu}\leq\frac{T}{1-\theta}\left(-R_{-\epsilon}(\hat{y},\hat{p})\right)^+. \tag{2.21}$$

Step 5 (The case $\hat{t}=0$). Now, let us consider the case in which $\hat{t}=0$. Since $\Delta_{\delta,\nu}>0$, $1-\theta>0$ and $0\leq t/T<1$,

$$\begin{aligned}\sup_{(x,t)\in Q_{T,\nu}}\psi(x,t;x,t)&\geq\sup_{(x,t)\in Q_{T,\nu}}\left(u(x,t)-v(x,t)-\frac{\delta}{\Psi_\nu(x,t)}\right)-(1-\theta)\,\Delta_{\delta,\nu}\\&=\Delta_{\delta,\nu}+|\,u-v\,|_{-,\Omega_{VT},0}-(1-\theta)\,\Delta_{\delta,\nu}\\&=\theta\,\Delta_{\delta,\nu}+|\,u-v\,|_{-,\Omega_{VT},0}.\end{aligned}$$

Therefore,

$$\begin{aligned}\theta\,\Delta_{\delta,\nu}+|\,u-v\,|_{-,\Omega_{VT},0}&\leq\psi(\hat{x},0;\hat{y},\hat{s})\\&\leq u(\hat{x},0)-v(\hat{y},\hat{s})-\frac{\hat{s}^2}{2\epsilon_t}-\frac{|\hat{x}-\hat{y}|^2}{2\epsilon_x}\\&\leq|\,u-v\,|_{-,\Omega,0}+v(\hat{x},0)-v(\hat{y},\hat{s})-\frac{\hat{s}^2}{2\epsilon_t}-\frac{|\hat{x}-\hat{y}|^2}{2\epsilon_x},\end{aligned}$$

and finally, since $\Delta_{\delta,\nu}>0$, $\hat{x}=\hat{y}+\epsilon_x\,\hat{p}_y$ and $|\,u-v\,|_{-,\Omega,0}\leq|\,u-v\,|_{-,\Omega_{VT},0}$, we obtain

$$\Delta_{\delta,\nu}\leq\frac{1}{\theta}\left(-\omega_{-\epsilon}(v;\hat{y},\hat{s},\hat{p})\right)^+. \tag{2.22}$$

Step 6 (Conclusion). Putting together the bounds (2.21) and (2.22) yields

$$\Delta_{\delta,\nu}\leq\max\left\{\frac{A}{\theta},\frac{B}{1-\theta}\right\},$$

where

$$A=\left(-\omega_{-\epsilon}(v;\hat{y},\hat{s},\hat{p})\right)^+\quad\text{and}\quad B=T\,\left(-R_{-\epsilon}(\hat{y},\hat{p})\right)^+.$$

Now, we easily see that

$$\Delta_{\delta,\nu}\leq A+B,$$

by taking the limit as θ tends to $A/(A+B)\in[0,1]$. This implies that (2.17) holds with $C=A+B$ and Theorem 2.2 follows.

3. Numerical experiments

The purpose of this section is to study the application of the a posteriori error estimate to approximations generated through numerical schemes; we consider a standard monotone scheme. Since the error estimate gives only an upper bound for the L^∞-norm of the difference between the viscosity solution u and any approximation v, we are going to numerically study its sharpness on several prototypical

one-dimensional problems. In other words, we are going to study how close the so-called *effectivity index* is to 1, which is defined as

$$ei(u,v) = \frac{\Phi(v;T,\Omega)}{\| u(T) - v(T) \|_{L^\infty(\Omega)}}, \tag{3.23}$$

where Ω is an arbitrary sub-domain of $\mathbb{R}^d$. In the case when $\Omega = \mathbb{R}^d$ or $\Omega = \Omega^{per}$, where Ω^{per} is a sub-domain of $\mathbb{R}^d$ that is equal in size to the period of the viscosity solution u, we obtain the *effectivity index* for the global a posteriori error estimate. To ease the notation we use $\mathcal{D}$ to denote the domain over which we estimate the a posteriori error estimates, i.e., $\mathcal{D} = Q_T$ in the case of the local a posteriori error estimate with the trapezoid as the domain, $\mathcal{D} = \Gamma_{\Omega,T}$ in the case of the local estimate with Q_T replaced by $\Gamma_{\Omega,T}$ as explained in the previous section, and $\mathcal{D} = \mathbb{R}^d \times (0,T)$ in the case of the global a posteriori error estimate. For the sake of simplicity, we use uniform grids in all our experiments.

3.1. **Discretization of the norms and the nonlinear functionals of the a posteriori error estimates.** Since the approximate solutions are defined by a finite number of degrees of freedom, we replace the domain $\mathcal{D}$ over which we evaluate the functionals $\Phi_\sigma(\cdot;\cdot,\cdot)$ by a finite number of points inside $\mathcal{D}$ which we denote by $\mathcal{D}_h$. We also replace the domain $\Omega \times \{T\}$ over which we evaluate the L^∞-norm of the difference between the viscosity solution u and its approximation v by a finite set of points in $\Omega \times \{T\}$ that we denote by $\Omega_{h,T}$.

Theoretically, the evaluation of the error estimates requires optimization over the set $\epsilon_x, \epsilon_t \in [0,\infty)$. In practice, however, it is sensible to replace $[0,\infty)$ with the set

$$\mathcal{E}_h = \{(\epsilon_x,\epsilon_t) = i \cdot (\omega_x/2, \omega_t/2)\,, 0 \le i \le 4 \,|\, \ln(1/\omega_x)\,|\}\,, \tag{3.24}$$

where ω_x, given by (3.31), is an upper bound for the artificial diffusion coefficient of the numerical scheme under consideration, and ω_t is given by

$$\omega_t = \frac{\omega_x}{\Delta x}\,\Delta t.$$

We denote by $\Phi_{h,\sigma}(\cdot)$ the functionals in the a posteriori error estimates obtained after the above mentioned modifications. To simplify the notation, we also let

$$\Phi_h(v) = \max_{\sigma\in\{-,+\}} \Phi_{h,\sigma}(v).$$

The effectivity index $ei(u,v)$ is accordingly replaced by the *computational effectivity index*

$$ei_h(u,v) = \Phi_h(v)/\| u - v \|_{L^\infty(\Omega_{h,T})}.$$

3.2. **Evaluation of the shifted residual on ∂Q_T.** Note that if (x,t) is a point on ∂Q_T, the paraboloid test could be satisfied by vectors $p = (p_x, p_t) \in \mathbb{R}^d \times \mathbb{R}$ that are not necessarily in the semi-differentials of v at (x,t), making the evaluation of the shifted residual a nontrivial matter. Consider the case when $\sigma = -$.

Recall that the set $\mathcal{A}_-(v;\epsilon)$ is the set of points $((x,t),p) \in \overline{Q_T} \times \mathbb{R}^{d+1}$ such that

$$v(y,s) \ge v(x,t) + p\cdot(y-x,s-t) - \frac{|\,s-t\,|^2}{2\epsilon_t} - \frac{|\,y-x\,|^2}{2\epsilon_x} \quad \forall (y,s) \in \overline{Q_T},$$

which implies that

$$\liminf_{(y,s)\to(x,t)} \frac{v(y,s) - v(x,t) - p\cdot(y-x,s-t)}{\|(y,s)-(x,t)\|} \ge 0 \quad \forall (y,s) \in \overline{Q_T}. \tag{3.25}$$

Let

$$\nu = \frac{(y,s)-(x,t)}{\|(y,s)-(x,t)\|}.$$

For simplicity assume that v is continuously differentiable in a neighborhood of the point (x,t), as is the case in many practical applications. In this case the two semi-differentials reduce to the exact differential of v and (3.25) implies that

$$(Dv(x,t)-p)\cdot\nu \geq 0, \tag{3.26}$$

which we can write as $\delta\cdot\nu\geq 0$ by letting $\delta=(Dv(x,t)-p)$. In particular, (3.26) holds for all ν that are inward normal to the boundary of the trapezoid ∂Q_T. Next, we show that in the case when H is a function of p only, as is the case in all our test problems, to compute the a posteriori error estimate, the shifted residual needs to be evaluated not at all points $((x,t),p)$ that pass the paraboloid test, but only at the points $((x,t),Dv(x,t))$. Indeed, assuming that H is differentiable in x and p, in (2.11) the term $(-R_{-\epsilon}(x,p))^+$ satisfies

$$\begin{aligned}(-R_{-\epsilon}(x,p))^+ &= (-[p_t+H(x+\epsilon_x p_x,p_x)])^+\\ &= (-[v_t(x,t)+H(x+\epsilon_x\nabla v(x,t),\nabla v(x,t))]+\Upsilon)^+\\ &\leq (-R_{-\epsilon}(x,\nabla v(x,t)))^+ + \Upsilon^+,\end{aligned}$$

where

$$\begin{aligned}\Upsilon &= -\delta_t - H\left(x+\epsilon_x(\nabla v(x,t)+\delta_x),\nabla v(x,t)+\delta_x\right)+H\left(x+\epsilon_x\nabla v(x,t),\nabla v(x,t)\right)\\ &= -\delta_t - \int_0^1 \frac{d}{d\eta}H\left(x+\epsilon_x(\nabla v(x,t)+\eta\,\delta_x),\nabla v(x,t)+\eta\,\delta_x\right)d\eta\\ &= -\delta_t - \int_0^1 \delta_x\cdot\epsilon_x\,\partial_x H\left(x+\epsilon_x(\nabla v(x,t)+\eta\,\delta_x),\nabla v(x,t)+\eta\,\delta_x\right)d\eta\\ &\quad - \int_0^1 \delta_x\cdot\partial_p H\left(x+\epsilon_x(\nabla v(x,t)+\eta\,\delta_x),\nabla v(x,t)+\eta\,\delta_x\right)d\eta.\end{aligned}$$

In the case when H is a differentiable function of p only, Υ reduces to

$$\begin{aligned}\Upsilon &= -\delta\cdot\left(1,\int_0^1 \partial_p H\left(x+\epsilon_x(\nabla v(x,t)+\eta\,\delta_x),\nabla v(x,t)+\eta\,\delta_x\right)d\eta\right)\\ &\leq 0,\end{aligned}$$

where in the second inequality we have used (3.26) and the definition of the boundary of Q_T. Therefore, $(-R_{-\epsilon}(x,p))^+$ is bounded above by $(-R_{-\epsilon}(x,\nabla v(x,t)))^+$.

3.3. **Fast evaluation of the paraboloid test.** To evaluate the paraboloid test (2.12) is computationally very expensive. To determine if the point $((x,t),p)\in\mathcal{D}\times\mathbb{R}^{d+1}$ belongs to the set $\mathcal{A}_\sigma(v;\epsilon)$, we must compare $P_v(x,t,p,(\sigma/\epsilon_x,\sigma/\epsilon_t)\,;\,y,s)$ and $v(y,s)$ for each point $(y,s)\in\mathcal{D}$. When v is Lipschitz, however, which is the case in most practical applications, it is not necessary to perform this comparison for all (y,s) in the domain $\mathcal{D}$, but only on a significantly smaller set. Note that if P_v is "tangent" to v at the point (y,s), we must have that

$$q=(q_x,q_t)=\left(p_x+\frac{\sigma}{\epsilon_x}(y-x),p_t+\frac{\sigma}{\epsilon_t}(s-t)\right)$$

for some $q \in D^\sigma v(y,s)$. This implies that

$$|\, y - x \,| = |\, p_x - q_x \,|\epsilon_x \leq 2\epsilon_x \| \, v(\cdot, s) \, \|_{\mathrm{Lip}(\mathcal{D}_{\cdot,s})} \tag{3.27}$$

and

$$|\, s - t \,| = |\, p_t - q_t \,|\epsilon_t \leq 2\epsilon_t \| \, v(y, \cdot) \, \|_{\mathrm{Lip}(\mathcal{D}_{y,\cdot})}, \tag{3.28}$$

where $\mathcal{D}_{\cdot,s} = \left\{ y \in \mathbb{R}^d \,|\, (y,s) \in \mathcal{D} \right\}$ and $\mathcal{D}_{y,\cdot} = \{ s \in (0,T) \,|\, (y,s) \in \mathcal{D} \}$. Thus, we can replace (2.12) by the following condition:

$$\sigma \left\{ v(y,s) - P_v(x,t,p,(\sigma/\epsilon_x, \sigma/\epsilon_t)\,;\, y, s) \right\} \leq 0 \qquad \forall (y,s) \in \mathcal{D} : (3.27),\ (3.28) \text{ hold.}$$

In our computations, we actually use a discrete version of the above paraboloid test, which is carried out only for (x,t), $(y,s) \in \mathcal{D}_h$.

3.4. **Test problems.** To study the efficiency of the global and local a posteriori error estimates, we consider the model problem

$$\begin{aligned} &u_t + H\,(u_x) = 0 && \text{for } (x,t) \in [-1,1] \times (0,\infty), \\ &u(-1,t) = u(1,t) && \text{for } t \in [0,\infty), \\ &u(x,0) = u_0(x) && \text{for } x \in [-1,1], \end{aligned} \tag{3.29}$$

with different Hamiltonian functions and initial conditions. Our test problems are chosen in order to cover the main cases of possible behavior of the viscosity solution. Thus, they display smooth and nonsmooth solutions for linear, convex, and nonconvex Hamiltonians; similar choices have been taken, for example, in [2, 6, 7, 14, 5]. With the notation that we introduced above, $\Omega^{per} = [-1,1]$. Table 1 summarizes the Hamiltonian functions $H(p)$, the initial conditions $u_0(x)$, the time intervals of consideration, and the smoothness of the viscosity solutions u at time T.

TABLE 1. Test problems.

Problem	$H(p)$	$u_0(x)$	$[0,T]$	$u(x,T)$
(L1)	$0.75p$	$\sin(\pi x)$	$[0, 0.15]$	smooth
(L2)	$0.75p$	$\begin{cases} 1 + \sin(0.5\pi x), & x \in [-1,0] \\ 0.5 + 0.5\cos(\pi x), & x \in (0,1] \end{cases}$	$[0, 0.15]$	nonsmooth
(C)	$0.5(p+1)^2$	$-\cos(\pi x)/\pi$	$[0, 0.20]$	smooth
			$[0, 0.40]$	nonsmooth
(NC)	$-\cos(p+1)$	$-\cos(\pi x)$	$[0, 0.5/\pi^2]$	smooth
			$[0, 1.5/\pi^2]$	nonsmooth

Note that problems (L1) and (L2), for which the Hamiltonian is a linear function, are examples of one-dimensional transport equations with constant coefficients, and their exact solutions are given by $u(x,t) = u_0\,(x - 0.75t)$. Furthermore, note that the spatial derivative of the viscosity solution of a first order one-dimensional Hamilton-Jacobi equation solves a corresponding conservation law. We can use the theory of characteristics and shock fitting [16] to obtain information about the shocks of the corresponding conservation laws. In this way we can find the location of the kinks in the viscosity solutions of our test problems at any time t. Figure 2 shows the exact solutions of the test problems at the end of the time intervals considered.

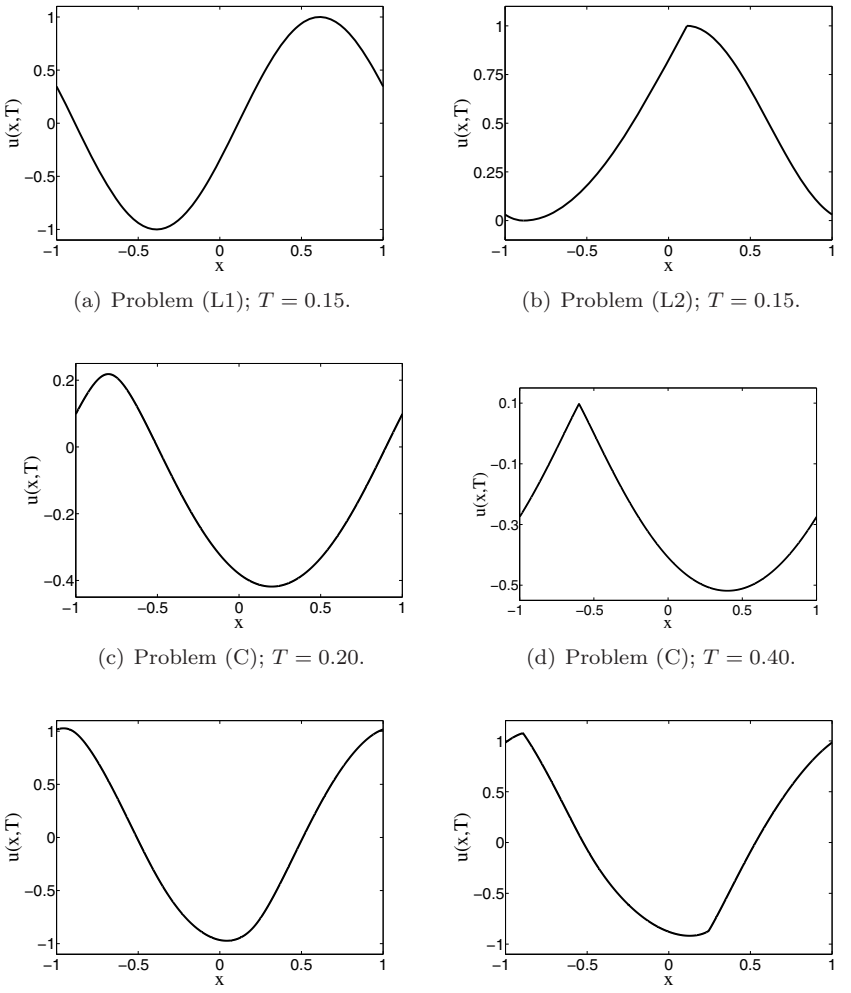

(a) Problem (L1); $T = 0.15$.

(b) Problem (L2); $T = 0.15$.

(c) Problem (C); $T = 0.20$.

(d) Problem (C); $T = 0.40$.

(e) Problem (NC); $T = 0.5/\pi^2$.

(f) Problem (NC); $T = 1.5/\pi^2$.

FIGURE 2. Exact solutions of the test problems.

3.5. **The monotone scheme.** In our numerical experiments we use a monotone scheme on a uniform grid. Given the mesh sizes Δx, $\Delta t > 0$, the value of our numerical approximation to the viscosity solution u of (3.29) at $(x_j, t_n) = (j\Delta x, n\Delta t)$, $j, n \in \mathbb{Z}$, will be denoted by v_j^n. We use the following scheme

$$v_j^{n+1} = v_j^n - \Delta t \left[H\left(\frac{v_{j+1}^n - v_{j-1}^n}{2\Delta x} \right) - \frac{\theta}{\lambda} \left(\frac{v_{j+1}^n - 2v_j^n + v_{j-1}^n}{\Delta x} \right) \right], \tag{3.30}$$

where $\theta > 0$ is given and $\lambda = \Delta t/\Delta x$. This scheme is monotone as long as $1 - 2\theta \geq 0$ (monotonicity in v_j^n), and $\theta - \lambda |\, H'(\alpha)\,|/2 \geq 0$ for $\alpha \in \mathbb{R}$ (monotonicity in v_{j+1}^n and

v_{j-1}^n) [9]. In equation (3.30), we take

$$\theta = \lambda \sup_{\alpha \in \mathbb{R}} \frac{|\, H'(\alpha)\,|}{2},$$

and fix λ in such a way that $1-2\theta \geq 0$ holds. This choice of θ yields the well-known Lax-Friedrichs scheme. The use of the scheme (3.30) is justified by the fact that it is guaranteed to converge to the correct viscosity solution [9]. Its downside is that it is at most first order accurate. If we let

$$\omega_x = \sup_{\alpha \in \mathbb{R}} \frac{|\, H'(\alpha)\,|}{2} \Delta x, \tag{3.31}$$

we can rewrite (3.30) as

$$\frac{v_j^{n+1} - v_j^n}{\Delta t} + H\left(\frac{v_{j+1}^n - v_{j-1}^n}{2\Delta x}\right) = \omega_x \left(\frac{v_{j+1}^n - 2v_j^n + v_{j-1}^n}{\Delta x^2}\right),$$

which is a discretized version of the Hamilton-Jacobi equation with an artificial viscosity term added, and ω_x allows the artificial viscosity to scale with the discretization.

The a posteriori error estimate (2.10) is based on the notion of viscosity solutions and so requires the comparison between continuous functions. We choose v to be the piecewise bilinear interpolant of the numerical solution given by the above scheme at the points (x_j, t_n). We then sample at the points $(x_{j+1/2}, t_{n+1/2})$, where $x_{j+1/2} = (x_{j+1} + x_j)/2$ and $t_{n+1/2} = (t_{n+1} + t_n)/2$. At the points $(x_{j+1/2}, t_{n+1/2})$ we have

$$\begin{aligned}
v(x_{j+1/2}, t_{n+1/2}) &= \frac{1}{4}\left(v_{j+1}^{n+1} + v_j^{n+1} + v_{j+1}^n + v_j^n\right), \\
v_x(x_{j+1/2}, t_{n+1/2}) &= \frac{1}{2\Delta x}\left(v_{j+1}^{n+1} - v_j^{n+1} + v_{j+1}^n - v_j^n\right), \\
v_t(x_{j+1/2}, t_{n+1/2}) &= \frac{1}{2\Delta t}\left(v_{j+1}^{n+1} - v_{j+1}^n + v_j^{n+1} - v_j^n\right).
\end{aligned}$$

Choosing the computational domain $\mathcal{D}_h$ as the sets of points $(x_{j+1/2}, t_{n+1/2})$ that lie inside $\mathcal{D}$, i.e., defining $\mathcal{D}_h$ as

$$\mathcal{D}_h = \left\{(x_{j+1/2}, t_{n+1/2}) \text{ for } j, n \in \mathbb{Z} \,|\, (x_{j+1/2}, t_{n+1/2}) \in \mathcal{D}\right\}$$

leads to well-defined derivatives of v at the points where the solution is sampled. Hence, at these points the semi-differentials are both nonempty, and $p = (p_x, p_t)$ is exactly the differential of v, i.e.,

$$D^- v(x_{j+1/2}, t_{n+1/2}) = D^+ v(x_{j+1/2}, t_{n+1/2}) = (v_x, v_t)\,(x_{j+1/2}, t_{n+1/2}).$$

As the computational domain $\Omega_{h,T}$ over which we evaluate the L^∞-norm of the difference between the viscosity solution u and the approximation v when we calculate the effectivity index, we take the union of the sets of points $\{(x_j, T) \mid x_j \in \Omega\}$ and $\left\{(x_{j+1/2}, T) \mid x_{j+1/2} \in \Omega\right\}$.

Note that calculating the upper bound for the artificial diffusion coefficient ω_x in the monotone scheme involves finding the supremum of $|\, H'(\alpha)\,|$ over all $\alpha \in \mathbb{R}$. It is easily seen that for problems (L1)-(L2) and (NC), $\sup_{\alpha \in \mathbb{R}} |\, H'(\alpha)\,|$ is equal to 0.75 and 1, respectively. For problem (C), however, $\sup_{\alpha \in \mathbb{R}} |\, H'(\alpha)\,|$ is not finite.

In this case, we take

$$\omega_x = \sup_{x\in\mathbb{R}} \frac{|\, H'\left(u_0'(x)\right)\,|}{2}\Delta x = \Delta x.$$

In the numerical experiments we obtain $|\, H'\left(v_x\left(x_{j+1/2}, t_{n+1/2}\right)\right)\,| < 2$ for all the points from the computational domain, so that the monotonicity condition is preserved and the above choice for ω_x is justified.

Also, recall that in one space dimension, the parameter V used in the determination of the region enclosed by the trapezoid Q_T is given by

$$V = \sup_{\substack{p_x, q_x\in\mathbb{R}\\ p_x\neq q_x}} \frac{|\, H(p_x) - H(q_x)\,|}{|\, p_x - q_x\,|},$$

where the right-hand side is assumed to be finite. V is equal to 1 and 0.75 for problems (L1)-(L2) and (NC), respectively. In the numerical experiments for problem (C) we take

$$V = \sup_{(x_{j+1/2}, t_{n+1/2})\in\mathcal{D}_h^{per}} |\, H'\left(v_x\left(x_{j+1/2}, t_{n+1/2}\right)\right)\,|,$$

where $\mathcal{D}_h^{per}$ is the set of points $(x_{j+1/2}, t_{n+1/2})$ that lie inside $\Omega^{per}\times(0,T)$, i.e.,

$$\mathcal{D}_h^{per} = \left\{(x_{j+1/2}, t_{n+1/2}) \text{ for } j,n\in\mathbb{Z}\,|\,(x_{j+1/2}, t_{n+1/2})\in\Omega^{per}\times(0,T)\right\}.$$

3.6. **Approximation of the domain $\Gamma_{\Omega,T}$.** To approximate the domain $\Gamma_{\Omega,T}$ introduced in Remark 5 right after our main theoretical result, Theorem 2.2, we proceed as suggested therein as follows.

Consider the terminal-value problem

$$\begin{aligned} &\phi_t + H'(u_x)\,\phi_x = 0 \qquad \text{for } (x,t)\in\mathbb{R}\times(0,T),\\ &\phi(x,T) = \begin{cases} 1 & \text{for } x\in\Omega,\\ 0 & \text{for } x\notin\Omega, \end{cases} \end{aligned} \tag{3.32}$$

where $\Omega\in\mathbb{R}$ and u is the viscosity solution of any of our test problems.

We solve this problem backwards using a monotone scheme on the computational domain $\mathcal{D}_h^{per}$ that we described above. To simplify the notation, set $y_j := x_{j+1/2}$ and $s_n := t_{n+1/2}$. The numerical approximation to the solution of (3.32) at the points (y_j, s_n) will be denoted by $\phi_h(y_j, s_n)$ or ϕ_j^n. The monotone scheme that we use to solve (3.32) is

$$\phi_j^n = \phi_j^{n+1} + \Delta t\left[H'\left(v_x\left(y_j, s_{n+1}\right)\right)\frac{\phi_{j+1}^{n+1} - \phi_{j-1}^{n+1}}{2\Delta x} + \omega_\phi\,\frac{\phi_{j+1}^{n+1} - 2\phi_j^{n+1} + \phi_{j-1}^{n+1}}{\Delta x^2}\right],$$

where v is the approximate solution described in the previous section and where

$$\omega_\phi = \sup_{(y_j,s_n)\in\mathcal{D}_h^{per}} \frac{|\, H'\left(v_x\left(y_j, s_n\right)\right)\,|}{2}\Delta x.$$

The monotone scheme adds an artificial diffusion term to equation (3.32), which causes the numerical approximation to $\phi(x,t)$ to be nonzero in a domain that is larger than the domain $\Gamma_{\Omega,T}$. To illustrate the effect of the artificial diffusion term with a simpler example, consider the equation

$$\rho_t = 0 \qquad \text{for } (x,t)\in\mathbb{R}\times(0,T), \tag{3.33}$$

with the terminal condition

$$\rho(x,T) = \begin{cases} 1 & \text{for } x \le 0, \\ 0 & \text{for } x > 0. \end{cases}$$

Trivially, the solution is $\rho(x,t) = \rho(x,T)$ for all $t \in (0,T)$. For $\kappa > 0$, the solution to

$$\rho_t^d = \kappa \rho_{xx}^d \qquad \text{for } (x,t) \in \mathbb{R} \times (0,T), \tag{3.34}$$

with the same terminal condition, however, is given by

$$\rho^d(x,t) = \frac{1}{2} - \frac{1}{2}\ \mathrm{Erf}\left(\frac{x}{\sqrt{4\kappa(T-t)}}\right), \quad \text{where} \quad \mathrm{Erf(x)} = \frac{2}{\sqrt{\pi}} \int_0^x e^{-p^2}\, dp.$$

Thus, the solution to the equation with the added diffusion term is monotonically decreasing and nonzero for all $-\infty < x < \infty$. Therefore, if we want to approximate the sub-domain of $\mathbb{R}$, in which the solution to (3.33) is nonzero by considering the solution to (3.34), we have to ignore the sub-domain of $\mathbb{R}$, in which the solution to (3.34) is "relatively" small.

We define our approximation to the domain $\Gamma_{\Omega,T}$ in a similar fashion. Let us denote this approximation by $\Gamma_{h,\Omega,T}$. At each time level n of $\mathcal{D}_h^{per}$ we let

$$r_n = \rho^d\left(\omega_\phi, s_n\right) / \sup_{y \in \mathbb{R}} \rho^d(y, s_n) = \rho^d\left(\omega_\phi, s_n\right)$$

and define $\Gamma_{h,\Omega,T}$ as

$$\Gamma_{h,\Omega,T} = \left\{ (y_j, s_n) \text{ for } j,n \in \mathbb{Z} \,|\, \phi_h(y_j, s_n) > r_n \sup_{y'} \phi_h(y', s_n), (y', s_n) \in \mathcal{D}_h^{per} \right\}.$$

The fact that the method described above approximates the domain $\Gamma_{\Omega,T}$ reasonably well in practice is illustrated by our numerical experiments.

3.7. **Numerical results.**

3.7.1. *The global a posteriori error estimate.* We show the results for the computational effectivity indexes for smooth solutions of problems (L1), (C), and (NC) in Figures 3(a),(c),(e). We see that in each of the three problems, the monotone scheme converges linearly, as expected, and that the computational effectivity index is independent of the mesh size Δx. In all of these cases, the values of the parameters ϵ_x and ϵ_t that minimize the nonlinear functional of the error estimate are equal to 0, in agreement with our discussion in section 2. The results when the exact solutions of our test problems are nonsmooth are shown in Figures 3(b),(d),(f). We can see that even for a nonsmooth viscosity solution the computational effectivity index for a linear Hamiltonian is nearly optimal. For problems (C) and (NC), the computational effectivity indexes increase faster as we decrease the mesh size Δx. Even in these cases, however, the computational effectivity indexes remain relatively small in magnitude and are proportional to $|\log(\Delta x)|$.

In Table 2 we show the optimal values of the auxiliary parameter $\epsilon = (\epsilon_x, \epsilon_t)$ for problems (L2), (C), and (NC), when the viscosity solutions are nonsmooth. In the third column, we show on how many values of $\epsilon = (\epsilon_x, \epsilon_t)$ the nonlinear functional of the error estimate has to be evaluated before hitting its minimum. The last column shows the ratio of the optimal values of the auxiliary parameters to the largest values that we allow them to have in the set (3.24). A reasonable choice for

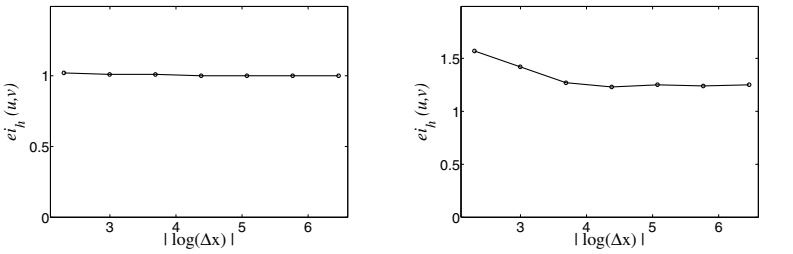

(a) Problem (L1): smooth solution (b) Problem (L2): nonsmooth solution

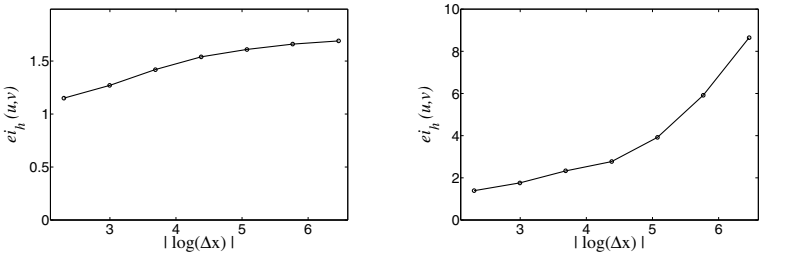

(c) Problem (C): smooth solution (d) Problem (C): nonsmooth solution

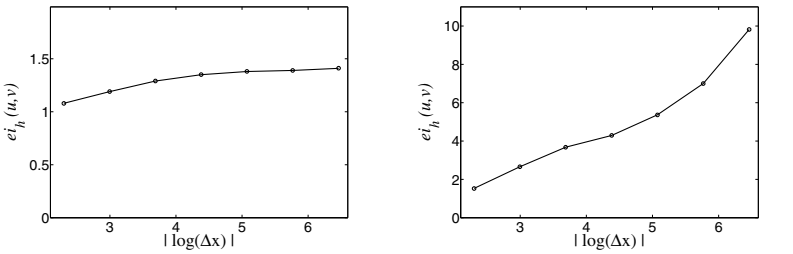

(e) Problem (NC): smooth solution (f) Problem (NC): nonsmooth solution

FIGURE 3. Computational effectivity index as a function of $|\log(\Delta x)|$.

the auxiliary parameters would result in a relatively stable ratio, as is the case for all test problems.

As we mentioned earlier, the paraboloid test can be used to detect the location of the kinks in the exact solutions. This fact is illustrated in Figure 4. We show the paths of the kinks in the viscosity solutions along with points from the computational domains $\mathcal{D}_h^{per}$ that fail the paraboloid test when the mesh size $\Delta x = 2/1280$. Note that even though the viscosity solution of problem (L2) is nonsmooth for all $t \in [0, T]$, we can capture the location of the kink for a certain period only. The reason is that the artificial diffusion term in the monotone scheme causes the approximate solution to "smooth out" as time increases, and after a certain point in time no points fail the paraboloid test near the kink in the viscosity solution. This can be overcome by considering a finer mesh.

At time $T = 0$, the kink in the viscosity solution of problem (L2) is at $x = 0$. For test problem (C), the location of the kink in the viscosity solution at time $T = 0.40$ is at $x = -0.60$, and for test problem (NC), the kinks in the viscosity solution at

TABLE 2. Parameter $\epsilon = (\epsilon_x, \epsilon_t)$ for **nonsmooth** exact solutions.

Problem	$2/\Delta x$ $(T/\Delta t)$	optimal (ϵ_x, ϵ_t)	ϵ-steps	ratio
(L2)	20 (10)	(0.00e+00, 0.00e+00)	0	0.00
	40 (20)	(4.69e–02, 7.03e–03)	5	0.31
	80 (40)	(3.28e–02, 4.92e–03)	7	0.37
	160 (80)	(2.11e–02, 3.16e–03)	9	0.41
	320 (160)	(1.52e–02, 2.29e–03)	13	0.52
	640 (320)	(1.05e–02, 1.58e–03)	18	0.67
	1280 (640)	(7.32e–03, 1.10e–03)	25	0.83
(C)	20 (10)	(0.00e+00, 0.00e+00)	0	0.00
	40 (20)	(1.00e–01, 4.00e–02)	4	0.33
	80 (40)	(7.50e–02, 3.00e–02)	6	0.40
	160 (80)	(4.38e–02, 1.75e–02)	7	0.39
	320 (160)	(3.13e–02, 1.25e–02)	10	0.48
	640 (320)	(2.34e–02, 9.38e–03)	15	0.63
	1280 (640)	(1.64e–02, 6.56e–03)	21	0.81
(NC)	20 (10)	(0.00e+00, 0.00e+00)	0	0.00
	40 (20)	(0.00e+00, 0.00e+00)	0	0.00
	80 (40)	(1.88e–02, 2.85e–03)	3	0.17
	160 (80)	(1.56e–02, 2.37e–03)	5	0.24
	320 (160)	(9.38e–03, 1.42e–03)	6	0.25
	640 (320)	(7.03e–03, 1.07e–03)	9	0.35
	1280 (640)	(5.08e–03, 7.72e–04)	13	0.45

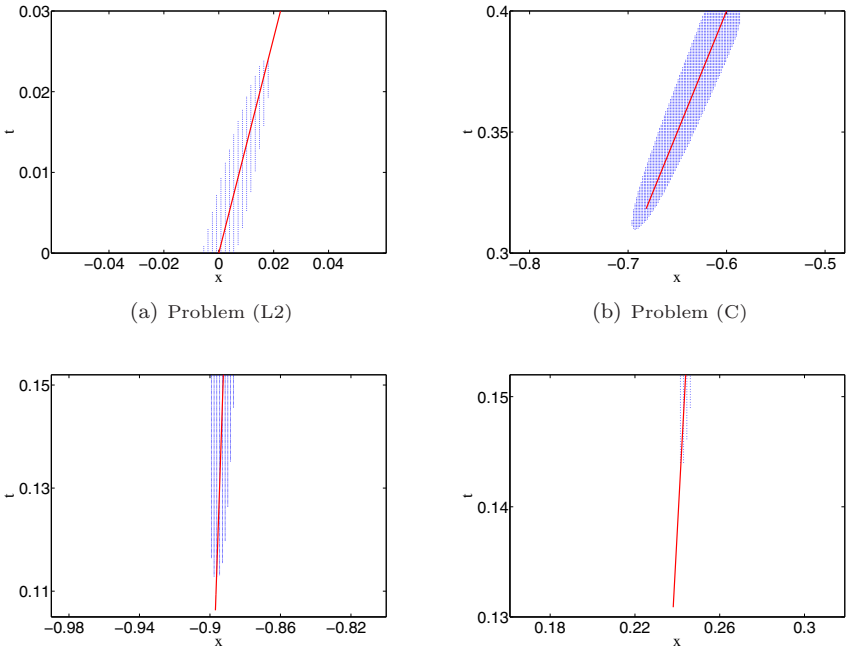

(a) Problem (L2)

(b) Problem (C)

(c) Problem (NC); kink 1

(d) Problem (NC); kink 2

FIGURE 4. Grid points that fail the paraboloid test around the kinks when $2/\Delta x = 1280$.

time $T = 1.5/\pi^2$ are at $x_1 = -0.8930$ and $x_2 = 0.2438$. Table 3 shows the interval $[a, b]$ at the first time level in the computational domain for problem (L2) and the last time level for problems (C) and (NC) over which the paraboloid test fails, i.e., the interval containing the set of points for which condition (2.12) is not satisfied.

We can see that as we refine the mesh, more points fail the paraboloid test, and the interval $[a, b]$ gets smaller. Note that for problem (C) we are able to capture the location of the kink even for a relatively coarse mesh. The kinks in the exact solution of problem (NC) are not as "pointed" as the kink in problem (C) (see Figures 2(d),(f)). Because of this fact, we are not able to capture the location of the kinks when we use very coarse meshes.

TABLE 3. **Paraboloid test**: the interval $[a, b]$ for which the paraboloid test fails at the first time level of the computational domain for problem (L2) and the last time level for problems (C) and (NC); the number of grid points in the interval $[a, b]$.

Problem	$2/\Delta x$	a	b	number of points inside $[a,b]$
(L2)	40	-0.0500	0.0500	2
	80	-0.0250	0.0250	2
	160	-0.0125	0.0250	3
	320	-0.0125	0.0125	4
	640	-0.0094	0.0094	6
	1280	-0.0063	0.0063	8
(C)	40	-0.7500	-0.6000	3
	80	-0.7000	-0.5750	5
	160	-0.6625	-0.5750	7
	320	-0.6438	-0.5750	11
	640	-0.6344	-0.5813	17
	1280	-0.6219	-0.5859	23
(NC)	80	-0.9250	-0.8750	2
kink 1	160	-0.9125	-0.8750	3
	320	-0.9063	-0.8813	4
	640	-0.9031	-0.8844	6
	1280	-0.9000	-0.8859	9
(NC)	640	0.2406	0.2469	2
kink 2	1280	0.2406	0.2469	4

3.7.2. *The local a posteriori error estimate.* In this section we study the efficiency of the local a posteriori error estimate with $Q_{h,T}$ and $\Gamma_{h,\Omega,T}$ as the computational domains when applied to problems (L2), (C), and (NC).

Test problem (L2). For problem (L2) we consider the intervals $[-0.15, 0.00]$, $[0.00, 0.15]$, and $[0.30, 0.45]$ at time $T = 0.15$. The viscosity solution has a kink inside the interval $[0.00, 0.15]$. It is smooth inside the interval $[-0.15, 0.00]$, but the region enclosed by its corresponding trapezoid Q_T contains a part of the path of the kink. The viscosity solution is smooth inside the interval $[0.30, 0.45]$, as well as inside its corresponding trapezoid Q_T.

We show the regions enclosed by the trapezoids Q_T corresponding to these intervals together with the characteristics that hit the intervals exactly at their endpoints and the sets of points from $\Gamma_{h,\Omega,T}$ when $\Delta x = 2/160$ in Figures 5(a),(c),(e). We see that the method described earlier gives a set of points $\Gamma_{h,\Omega,T}$ that almost perfectly matches the set of points from $\mathcal{D}_h^{per}$ that lie inside $\Gamma_{\Omega,T}$.

Figures 5(b),(d),(f) show the computational effectivity indexes as functions of $|\log(\Delta x)|$ when $Q_{h,T}$ and $\Gamma_{h,\Omega,T}$ are used as the computational domains of dependence.

As expected, for both computational domains the smallest effectivity indexes are obtained for the interval $[0.30, 0.45]$; the viscosity solution is smooth both inside the interval at time T and inside the trapezoid Q_T. When Q_T is used, the error estimate

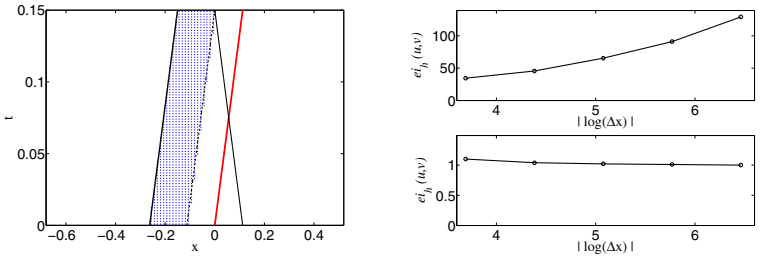

(a) $\Omega = [-0.15, 0.00]$ (b) top: $Q_{h,T}$; bottom: $\Gamma_{h,\Omega,T}$

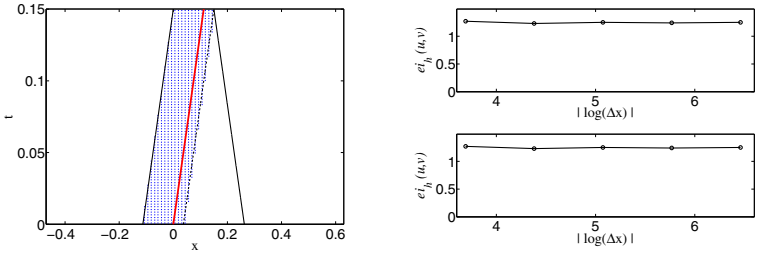

(c) $\Omega = [0.00, 0.15]$ (d) top: $Q_{h,T}$; bottom: $\Gamma_{h,\Omega,T}$

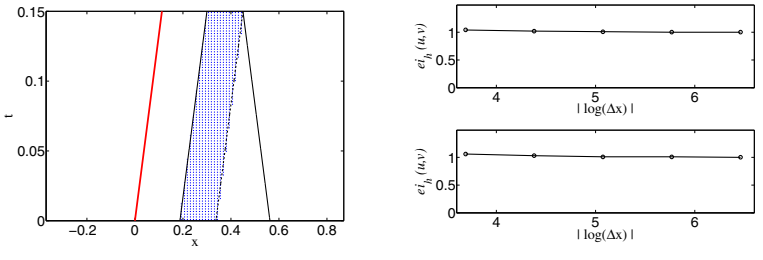

(e) $\Omega = [0.30, 0.45]$ (f) top: $Q_{h,T}$; bottom: $\Gamma_{h,\Omega,T}$

FIGURE 5. **Problem (L2)**; (a),(c),(e): trapezoid Q_T (legs are given by the solid black lines); characteristics that hit the interval Ω exactly at the endpoints (dashed lines; left one coincides with the left leg of Q_T); path of the kink (red line); points from $\Gamma_{h,\Omega,T}$ when $\Delta x = 2/160$); (b), (d), (e): computational effectivity index as a function of $|\log(\Delta x)|$.

has the largest computational effectivity index for the interval $[-0.15, 0.00]$, where the viscosity solution is smooth, but whose corresponding Q_T contains a part of the path of the kink. Replacing $Q_{h,T}$ by $\Gamma_{h,\Omega,T}$ significantly improves the efficiency of the error estimate in this case. For both computational domains, the computational effectivity index remains relatively small and close to 1 for the interval $[0.00, 0.15]$, where the viscosity solutions has a discontinuous derivative.

Table 4 contains information about the optimal values of the auxiliary parameters ϵ_x and ϵ_t for both computational domains $Q_{h,T}$ and $\Gamma_{h,\Omega,T}$. The ratio of the optimal auxiliary parameters to the maximum values allowed by the set (3.24) remains stable as the mesh size decreases by a few orders of magnitude, confirming that we have suitably chosen the set for the parameters. As expected, the optimal

values of the auxiliary parameters ϵ_x and ϵ_t are 0 when the exact solution is smooth inside the interval Ω and the domains Q_T and $\Gamma_{\Omega,T}$.

TABLE 4. Parameter $\epsilon = (\epsilon_x, \epsilon_t)$ for problem (L2).

Interval	Computational domain	$2/\Delta x$ $(T/\Delta t)$	optimal (ϵ_x, ϵ_t)	ϵ-steps	ratio
[-0.15, 0.00]	$Q_{h,T}$	80 (40)	(3.28e–02, 4.92e–03)	7	0.37
		160 (80)	(2.11e–02, 3.16e–03)	9	0.41
		320 (160)	(1.52e–02, 2.29e–03)	13	0.52
		640 (320)	(1.05e–02, 1.58e–03)	18	0.67
		1280 (640)	(7.32e–03, 1.10e–03)	25	0.83
[0.00, 0.15]	$Q_{h,T}$	80 (40)	(3.28e–02, 4.92e–03)	7	0.37
		160 (80)	(2.11e–02, 3.16e–03)	9	0.41
		320 (160)	(1.52e–02, 2.29e–03)	13	0.52
		640 (320)	(1.05e–02, 1.58e–03)	18	0.67
		1280 (640)	(7.32e–03, 1.10e–03)	25	0.83
[0.00, 0.15]	$\Gamma_{h,\Omega,T}$	80 (40)	(3.28e–02, 4.92e–03)	7	0.37
		160 (80)	(2.11e–02, 3.16e–03)	9	0.41
		320 (160)	(1.52e–02, 2.29e–03)	13	0.52
		640 (320)	(1.05e–02, 1.58e–03)	18	0.67
		1280 (640)	(7.32e–03, 1.10e–03)	25	0.83

Test problem (C). For problem (C) we consider the intervals $[-0.90, -0.75]$, $[-0.70, -0.55]$, and $[0.00, 0.15]$ at $T = 0.40$. The viscosity solution has a discontinuous derivative in the interval $[-0.70, -0.55]$. In $[-0.90, -0.75]$, the viscosity solution is smooth; however, the region enclosed by its corresponding Q_T contains a part of the path of the kink in the viscosity solution. The solution is smooth inside the interval $[0.00, 0.15]$, as well as inside the trapezoid Q_T.

We show the regions enclosed by the trapezoids Q_T corresponding to these intervals and the sets of points from $\Gamma_{h,\Omega,T}$ when $\Delta x = 2/160$ in Figures 6(a),(c),(e). Again note that the set of points $\Gamma_{h,\Omega,T}$ matches the set of points from $\mathcal{D}_h^{per}$ that lie inside $\Gamma_{\Omega,T}$ almost perfectly for the intervals $[-0.90, -0.75]$ and $[-0.70, -0.55]$ and reasonably well for the interval $[0.00, 0.15]$. We show the results for the computational effectivity indexes in Figures 6(b),(d),(f).

The lowest computational effectivity indexes are obtained for the interval $[0.00, 0.15]$ for both domains, as expected. When $Q_{h,T}$ is used as the computational domain, the error estimate has the largest computational effectivity index for the interval $[-0.90, -0.75]$, where the viscosity solution is smooth, but whose corresponding Q_T contains a part of the path of the kink. The improvement in the computational effectivity index for this interval when we replace $Q_{h,T}$ by $\Gamma_{h,\Omega,T}$ as the computational domain is significant. The results for the interval $[-0.70, -0.55]$ that contains the kink in the viscosity solution are similar for both computational domains. The computational effectivity index for this interval is larger compared to the computational effectivity indexes for the intervals where the viscosity solution is smooth; however, it is still proportional to $|\log(\Delta x)|$. Table 5 shows the optimal values of the auxiliary parameters ϵ_x and ϵ_t.

Test problem (NC). For problem (NC) we consider five different intervals for which we compute the computational effectivity index when $T = 1.5/\pi^2$. The viscosity solution has a discontinuous derivative in the intervals $[-0.95, -0.80]$ and $[0.15, 0.30]$. In the intervals $[-0.88, -0.73]$ and $[0.08, 0.23]$, the viscosity solution is smooth; however, the regions enclosed by their corresponding trapezoids Q_T contain parts of the paths of the two kinks. Finally, the viscosity solution is smooth inside the interval $[-0.30, -0.15]$, as well as inside its corresponding Q_T. We show the

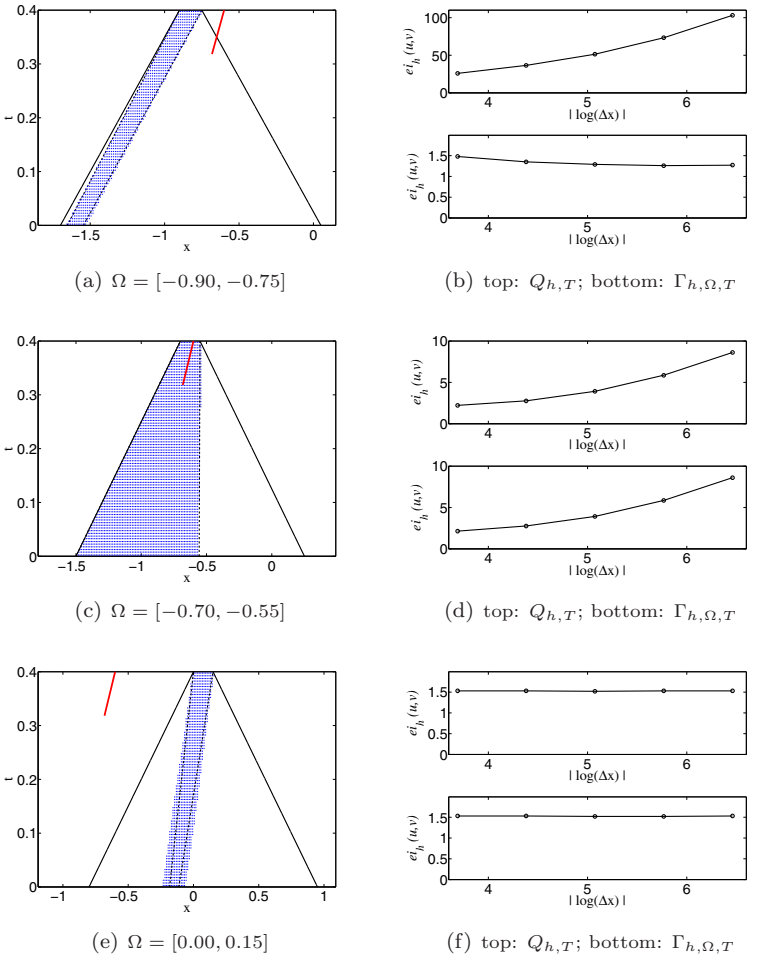

(a) $\Omega = [-0.90, -0.75]$ (b) top: $Q_{h,T}$; bottom: $\Gamma_{h,\Omega,T}$

(c) $\Omega = [-0.70, -0.55]$ (d) top: $Q_{h,T}$; bottom: $\Gamma_{h,\Omega,T}$

(e) $\Omega = [0.00, 0.15]$ (f) top: $Q_{h,T}$; bottom: $\Gamma_{h,\Omega,T}$

FIGURE 6. **Problem (C)**; (a),(c),(e): trapezoid Q_T (legs are given by the solid black lines); characteristics that hit the interval Ω exactly at the endpoints (dashed lines); path of the kink (red line); points from $\Gamma_{h,\Omega,T}$ when $\Delta x = 2/160$); (b), (d), (e): computational effectivity index as a function of $|\log(\Delta x)|$.

regions enclosed by the trapezoid Q_T and the sets of points from $\Gamma_{h,\Omega,T}$ for these intervals in Figures 7(a),(c),(e),(g),(i).

Figures 7(b),(d),(f),(h),(j) show the computational effectivity indexes as functions of $|\log(\Delta x)|$. The results are similar to the results for test problem (C). As expected, the smallest effectivity index is obtained in the cases when the viscosity solution is smooth in both the interval of consideration and inside its computational domain of dependence. The computational effectivity indexes for the intervals $[-0.95, -0.80]$ and $[0.15, 0.30]$ that contain the kinks in the viscosity solution are proportional to $|\log(\Delta x)|$ and remain reasonably small as we refine the mesh for both computational domains. The largest effectivity indexes are again obtained for the intervals where the viscosity solution is smooth, but whose corresponding

trapezoids Q_T contain parts of the path of the kinks in viscosity solution, i.e., the intervals $[-0.88, -0.73]$ and $[0.08, 0.23]$. Replacing $Q_{h,T}$ by $\Gamma_{h,\Omega,T}$ for these intervals results in significantly lower computational indexes that remain close to 1 throughout the large variation of the sizes of Δx and Δt.

TABLE 5. Parameter $\epsilon = (\epsilon_x, \epsilon_t)$ for problem (C).

Interval	Computational domain	$2/\Delta x$ $(T/\Delta t)$	optimal (ϵ_x, ϵ_t)	ϵ-steps	ratio
[-0.90, -0.75]	$Q_{h,T}$	80 (40)	(6.25e–02, 2.50e–02)	5	0.33
		160 (80)	(4.38e–02, 1.75e–02)	7	0.39
		320 (160)	(3.13e–02, 1.25e–02)	10	0.48
		640 (320)	(2.34e–02, 9.38e–03)	15	0.63
		1280 (640)	(1.64e–02, 6.56e–03)	21	0.81
[-0.70, 0.55]	$Q_{h,T}$	80 (40)	(7.50e–02, 3.00e–02)	6	0.40
		160 (80)	(4.38e–02, 1.75e–02)	7	0.39
		320 (160)	(3.13e–02, 1.25e–02)	10	0.48
		640 (320)	(2.34e–02, 9.38e–03)	15	0.63
		1280 (640)	(1.64e–02, 6.56e–03)	21	0.81
[-0.70, -0.55]	$\Gamma_{h,\Omega,T}$	80 (40)	(7.50e–02, 3.00e–02)	6	0.40
		160 (80)	(4.38e–02, 1.75e–02)	7	0.39
		320 (160)	(3.13e–02, 1.25e–02)	10	0.48
		640 (320)	(2.34e–02, 9.38e–03)	15	0.63
		1280 (640)	(1.64e–02, 6.56e–03)	21	0.81

TABLE 6. Parameter $\epsilon = (\epsilon_x, \epsilon_t)$ for problem (NC).

Interval	Computational domain	$2/\Delta x$ $(T/\Delta t)$	optimal (ϵ_x, ϵ_t)	ϵ-steps	ratio
[-0.95, -0.80]	$Q_{h,T}$	80 (40)	(2.50e–02, 3.80e–03)	4	0.22
		160 (80)	(1.56e–02, 2.37e–03)	5	0.24
		320 (160)	(1.09e–02, 1.66e–03)	7	0.29
		640 (320)	(7.81e–03, 1.19e–03)	10	0.38
		1280 (640)	(5.47e–03, 8.31e–04)	14	0.48
[-0.88, -0.73]	$Q_{h,T}$	80 (40)	(0.00e+00, 0.00e+00)	0	0.00
		160 (80)	(1.56e–02, 2.37e–03)	5	0.24
		320 (160)	(1.09e–02, 1.66e–03)	7	0.29
		640 (320)	(7.03e–03, 1.07e–03)	9	0.35
		1280 (640)	(5.08e–03, 7.72e–04)	13	0.45
[0.15, 0.30]	$Q_{h,T}$	80 (40)	(0.00e+00, 0.00e+00)	0	0.00
		160 (80)	(0.00e+00, 0.00e+00)	0	0.00
		320 (160)	(0.00e+00, 0.00e+00)	0	0.00
		640 (320)	(7.03e–03, 1.07e–03)	9	0.35
		1280 (640)	(5.08e–03, 7.72e–04)	13	0.45
[-0.95, -0.80]	$\Gamma_{h,\Omega,T}$	80 (40)	(2.50e–02, 3.80e–03)	4	0.22
		160 (80)	(1.56e–02, 2.37e–03)	5	0.24
		320 (160)	(1.09e–02, 1.66e–03)	7	0.29
		640 (320)	(7.81e–03, 1.19e–03)	10	0.38
		1280 (640)	(5.47e–03, 8.31e–04)	14	0.48
[0.15, 0.30]	$\Gamma_{h,\Omega,T}$	80 (40)	(0.00e+00, 0.00e+00)	0	0.00
		160 (80)	(0.00e+00, 0.00e+00)	0	0.00
		320 (160)	(0.00e+00, 0.00e+00)	0	0.00
		640 (320)	(7.03e–03, 1.07e–03)	9	0.35
		1280 (640)	(5.08e–03, 7.72e–04)	13	0.45

Table 6 contains the information about the optimal values of the auxiliary parameter $\epsilon = (\epsilon_x, \epsilon_t)$. The optimal values for ϵ_x and ϵ_t in the cases when the viscosity solution is smooth inside the intervals and inside the computational domains of dependence are 0, as expected. Note that, even though the region enclosed by the trapezoid Q_T corresponding to the interval $[0.08, 0.23]$ contains a part of the path of the kink in the viscosity solution, the values of the auxiliary parameters are equal to 0. The reason is that the kink inside Q_T is relatively "mild" (see Figure 2(f)).

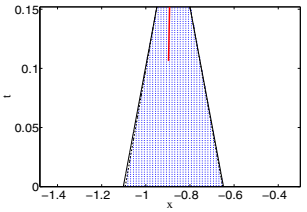

(a) $\Omega = [-0.95, -0.80]$

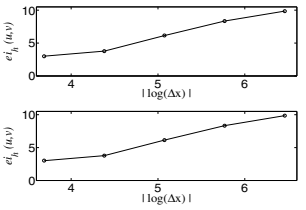

(b) top: $Q_{h,T}$; bottom: $\Gamma_{h,\Omega,T}$

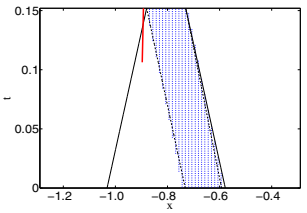

(c) $\Omega = [-0.88, -0.73]$

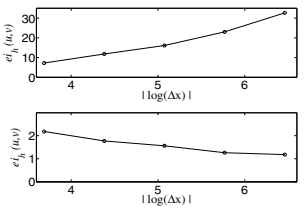

(d) top: $Q_{h,T}$; bottom: $\Gamma_{h,\Omega,T}$

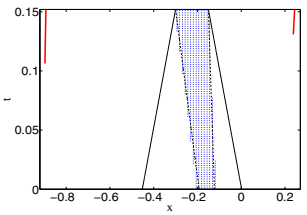

(e) $\Omega = [-0.30, -0.15]$

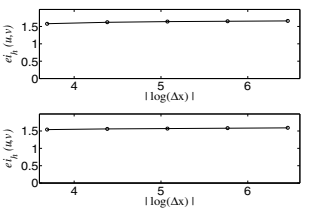

(f) top: $Q_{h,T}$; bottom: $\Gamma_{h,\Omega,T}$

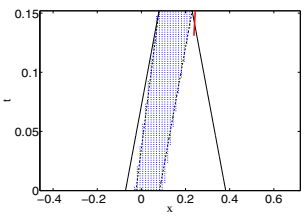

(g) $\Omega = [0.08, 0.23]$

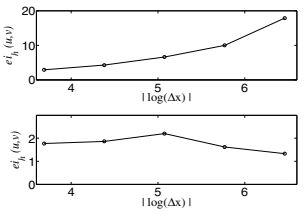

(h) top: $Q_{h,T}$; bottom: $\Gamma_{h,\Omega,T}$

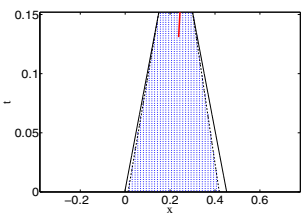

(i) $\Omega = [0.15, 0.30]$

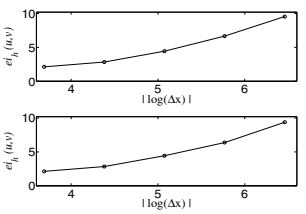

(j) top: $Q_{h,T}$; bottom: $\Gamma_{h,\Omega,T}$

FIGURE 7. **Problem (NC)**; (a),(c),(e): trapezoid Q_T (legs are given by the solid black lines); characteristics that hit the interval Ω exactly at the endpoints (dashed lines); path of the kink (red line); points from $\Gamma_{h,\Omega,T}$ when $\Delta x = 2/160$); (b), (d), (e): computational effectivity index as a function of $|\log(\Delta x)|$.

For the cases involving a kink in the exact solution, the ratio of the optimal auxiliary parameters to the maximum values that are allowed in the set (3.24) remains relatively stable as the mesh gets refined, indicating that this choice for the set of values for the parameters ϵ_x and ϵ_t is reasonable.

4. Concluding remarks

In this paper, we obtain a generalization of the global a posteriori error estimate for time-dependent Hamilton-Jacobi equations introduced in [3] that gives an upper bound for the difference at time T between the viscosity solution u of the Cauchy problem (1.1), (1.2) and a continuous function v for any sub-domain of $\mathbb{R}^d$. This allows us to define the first local a posteriori error estimate for time-dependent Hamilton-Jacobi equations.

We provide numerical experiments studying the efficiency of this local error estimate and the global a posteriori error estimate obtained in [3]. The numerical experiments confirm that even in the difficult cases of nonlinear Hamiltonians, when the viscosity solution displays kinks, the error estimates applied to a monotone scheme produce effectivity indexes that remain relatively small as the discretization parameters vary in several orders of magnitude. This shows that these a posteriori error estimates could be effectively used in adaptive algorithms with rigorous error control for time-dependent Hamilton-Jacobi equations, similar to the algorithms proposed in [5], [6], and [7] for steady-state Hamilton-Jacobi equations.

Two topics constitute the subject of ongoing research. The first is a theoretical justification of the use of the set $\Gamma_{\Omega,T}$ instead of the trapezoid Q_T in the a posteriori error estimate. The second is the extension of the estimates to high-order schemes. Note that the use of the a posteriori error estimate with formally high-order numerical schemes is likely to give rise to a suboptimal effectivity index just as for the steady-state case; see [2]. In [5], the estimate obtained in [2] had to be suitably modified before applied to high-order schemes like discontinuous Galerkin methods. It is thus reasonable to expect that a similar modification should be carried out in the time-dependent case also.

References

[1] R. Abgrall, *Numerical discretization of the first-order Hamilton-Jacobi equation on triangular meshes*, Comm. Pure Appl. Math. **49** (1996), 1339–1373. MR1414589 (98d:65121)

[2] S. Albert, B. Cockburn, D. French, and T. Peterson, *A posteriori error estimates for general numerical methods for Hamilton-Jacobi equations. Part I: The steady state case*, Math. Comp. **71** (2002), 49–76. MR1862988 (2002m:65107)

[3] ———, *A posteriori error estimates for general numerical methods for Hamilton-Jacobi equations. Part II: The time-dependent case*, Finite Volumes for Complex Applications, (R. Herbin and D. Kröner, eds.), vol. III, Hermes Penton Science, June 2002, 17–24. MR2007401

[4] T. Barth and J. Sethian, *Numerical schemes for Hamilton-Jacobi and level set equations on triangular domains*, J. Comput. Phys. **145** (1998), 1–40. MR1640142 (99d:65277)

[5] Y. Chen and B. Cockburn, *An adaptive high order discontinuous Galerkin method with error control for time Hamilton-Jacobi equations. Part I: The one-dimensional steady state case*, J. Comput. Phys. **226** (2007), 1027–1058. MR2356867 (2008k:65239)

[6] B. Cockburn and B. Yenikaya, *An adaptive method with rigorous error control for the Hamilton-Jacobi equations. Part I: The one-dimensional steady state case*, Appl. Numer. Math. **52** (2005), 175–195. MR2116910 (2005i:65200)

[7] ———, *An adaptive method with rigorous error control for the Hamilton-Jacobi equations. Part II: The two-dimensional steady state case*, J. Comput. Phys. **209** (2005), 391–405. MR2151991 (2006b:65185)

[8] M. G. Crandall, L. C. Evans, and P. L. Lions, *Some properties of viscosity solutions of Hamilton-Jacobi equations*, Trans. Amer. Math. Soc. **282** (1984), 478–502. MR732102 (86a:35031)

[9] M. G. Crandall and P. L. Lions, *Two approximations of solutions of Hamilton-Jacobi equations*, Math. Comp. **43** (1984), 1–19. MR744921 (86j:65121)

[10] M. Falcone and R. Ferretti, *Discrete time high-order schemes for viscosity solutions of Hamilton-Jacobi-Bellman equations*, Numer. Math. **67** (1994), 315–344. MR1269500 (95d:49045)

[11] C. Hu and C.-W. Shu, *A discontinuous Galerkin finite element method for Hamilton-Jacobi equations*, SIAM J. Sci. Comput. **21** (1999), 666–690. MR1718679 (2000g:65095)

[12] H. Ishii, *Uniqueness of unbounded viscosity solution of Hamilton-Jacobi equations*, Indiana Univ. Math. Journal **33** (1984), 721–748. MR756156 (85h:35057)

[13] S. Osher and C.-W. Shu, *High-order essentially nonoscillatory schemes for Hamilton-Jacobi equations*, SIAM J. Numer. Anal. **28** (1991), 907–922. MR1111446 (92e:65118)

[14] J. Qian, *Approximations for viscosity solutions of Hamilton-Jacobi equations with locally varying time and space grids*, SIAM J. Numer. Anal. **2006**, 2391–2401. MR2206440 (2007b:49055)

[15] P. E. Souganidis, *Approximation schemes for viscosity solutions of Hamilton-Jacobi equations*, J. Diff. Eqns. **59** (1985), 1–43. MR803085 (86k:35028)

[16] G. B. Whitham, *Linear and nonlinear waves*, Wiley, New York, NY, 1974. MR0483954 (58:3905)

School of Mathematics, University of Minnesota, 206 Church Street S.E., Minneapolis, Minnesota 55455

E-mail address: cockburn@math.umn.edu

School of Mathematics, University of Minnesota, 206 Church Street S.E., Minneapolis, Minnesota 55455

E-mail address: merev001@math.umn.edu

Department of Mathematics, Michigan State University, East Lansing, Michigan 48824

E-mail address: qian@math.msu.edu